RSC Advances

PAPER

View Article Online
View Journal | View Issue

Cite this: *RSC Adv.*, 2020, **10**, 32548

Metabolic characterisation of *Magnetospirillum gryphiswaldense* MSR-1 using LC-MS-based metabolite profiling†

Salah Abdelrazig, [a] Laudina Safo, [a] Graham A. Rance, [b] Michael W. Fay, [b] Eirini Theodosiou, [c] Paul D. Topham, [c] Dong-Hyun Kim *[a] and Alfred Fernández-Castané *[cd]

Magnetosomes are nano-sized magnetic nanoparticles with exquisite properties that can be used in a wide range of healthcare and biotechnological applications. They are biosynthesised by magnetotactic bacteria (MTB), such as *Magnetospirillum gryphiswaldense* MSR-1 (*Mgryph*). However, magnetosome bioprocessing yields low quantities compared to chemical synthesis of magnetic nanoparticles. Therefore, an understanding of the intracellular metabolites and metabolic networks related to *Mgryph* growth and magnetosome formation are vital to unlock the potential of this organism to develop improved bioprocesses. In this work, we investigated the metabolism of *Mgryph* using untargeted metabolomics. Liquid chromatography-mass spectrometry (LC-MS) was performed to profile spent medium samples of *Mgryph* cells grown under O_2-limited ($n = 6$) and O_2-rich conditions ($n = 6$) corresponding to magnetosome- and non-magnetosome producing cells, respectively. Multivariate, univariate and pathway enrichment analyses were conducted to identify significantly altered metabolites and pathways. Rigorous metabolite identification was carried out using authentic standards, the *Mgryph*-specific metabolite database and MS/MS mzCloud database. PCA and OPLS-DA showed clear separation and clustering of sample groups with cross-validation values of $R^2X = 0.76$, $R^2Y = 0.99$ and $Q^2 = 0.98$ in OPLS-DA. As a result, 50 metabolites linked to 45 metabolic pathways were found to be significantly altered in the tested conditions, including: glycine, serine and threonine; butanoate; alanine, aspartate and glutamate metabolism; aminoacyl-tRNA biosynthesis and; pyruvate and citric acid cycle (TCA) metabolisms. Our findings demonstrate the potential of LC-MS to characterise key metabolites in *Mgryph* and will contribute to further understanding the metabolic mechanisms that affect *Mgryph* growth and magnetosome formation.

Received 17th June 2020
Accepted 23rd August 2020

DOI: 10.1039/d0ra05326k

rsc.li/rsc-advances

1. Introduction

Magnetotactic bacteria (MTB) are a diverse group of microorganisms which are able to produce intracellular nano-sized crystals of magnetite (Fe_3O_4) or greigite (Fe_3S_4) bound to a cytoplasmic membrane and packed in a chain-like structure namely, the magnetosomes.[1] These biosynthesised magnetic nanoparticles present exquisite properties, such as exhibiting a narrow size distribution, ferrimagnetism, and high stability towards self-aggregation,[1,2] and they can be functionalised *in vivo* using genetic engineering tools.[3] Magnetosomes can be used in a wide range of biotechnological and biomedical applications, such as cancer therapy, magnetic resonance agents or bioremediation.[2,4–6] However, their real-world application is hindered to a large extent by the low availability of such materials.

Magnetospirillum gryphiswaldense MSR-1 (*Mgryph*) is an MTB that can be grown at relatively high cell densities and is capable of producing up to 4% of its dry cell weight in the form of magnetosomes.[7] *Mgryph* has been extensively used as an MTB model organism addressing genetics, physiology and magnetosome formation mechanism studies.[8] Recently, advances in *Mgryph* bioprocessing[9–11] and metabolic engineering[12] have resulted in an increase of magnetosome yields, thus, paving the way for future magnetosome production at a large scale. However, magnetosome formation occurs under tightly controlled growth conditions. For example, *Mgryph* synthesises magnetosomes in an O_2-limited environment as the

[a]*Centre for Analytical Bioscience, Advanced Materials and Healthcare Technologies Division, School of Pharmacy, University of Nottingham, Nottingham, NG7 2RD, UK. E-mail: dong-hyun.kim@nottingham.ac.uk; Tel: +44 (0)115 74 84697*

[b]*Nanoscale and Microscale Research Centre, University of Nottingham, Nottingham, NG7 2RD, UK*

[c]*Aston Institute of Materials Research, Aston University, Birmingham, B4 7ET, UK. E-mail: a.fernandez-castane1@aston.ac.uk; Tel: +44 (0)121 204 4870*

[d]*Energy and Bioproducts Research Institute, Aston University, Birmingham, B4 7ET, UK*

† Electronic supplementary information (ESI) available. See DOI: 10.1039/d0ra05326k

biomineralisation of the magnetite is only viable under microaerobic conditions.[3] The carbon source and its effect on cell growth and magnetosome formation have been widely studied in *Mgryph*.[3,11] However, the central carbon metabolism (CCM) of *Mgryph* and the regulation of its metabolic pathways during the formation of the magnetosome and the cell growth is poorly understood at the cellular level. CCM is known to provide biomass precursors and energy through a carbon flux into different biochemical reactions. Previous studies suggested that the production of magnetosomes is an energy-dependent process as the ATPase[13] and the magnetosome membrane protein MamK[14] were found to be involved in the ferrous uptake by the MTB. Moreover, the cyclic AMP (cAMP) receptor protein (CRP), which is a global transcriptional regulator in prokaryotes, was found to play an important role in energy metabolism and in the formation of magnetosomes.[15] However, further studies of the intermediates, such as the fluxes of the intracellular metabolites at different stages of the cell growth, and their complex networks, including CCM, by which magnetosomes are formed, remain unexplored in *Mgryph*. Such research can potentially enable unlocking of the mechanism whereby efficient cell growth and magnetosome production can be optimised.

Metabolomics using liquid chromatography-mass spectrometry (LC-MS) has the potential to provide an insight into cell metabolism and metabolic pathways.[16,17] For instance, LC-MS was successfully used to monitor the intracellular metabolites of *Clostridium autoethanogenum* during gas fermentation, which enabled the optimisation of biofuel production using computational modelling.[18] In addition, the growth medium analysis of bacterial cells using LC-MS provides comprehensive metabolic information which enables the study of the microenvironmental changes caused by the microbial activities under different culture conditions.[19] Since the analysis of the extracellular metabolites in a growth medium using LC-MS requires minimum sample preparation (no complicated cell quenching and extraction procedures), this technique was used successfully to monitor metabolic changes in the growth media analysed from *E. coli* cultures investigating the efficient fermentation of fucose for bio-based products,[20] and *Clostridium acetobutylicum* to study the use of polyketides to regulate cellular differentiation.[21] However, to the best of our knowledge, no LC-MS studies have been performed for the metabolic characterisation of *Mgryph*. This technique can be employed to monitor the CCM and determine the affected pathways linked to the production of magnetosomes by *Mgryph*.

In this study, we first characterised the physiological properties of *Mgryph* grown under O_2-limited and O_2-rich conditions in shake flask cultures. Then, we applied untargeted metabolomics using LC-MS for profiling and identification of metabolites in the growth media. This was done in order to investigate the significantly altered metabolites and pathways in *Mgryph*. Our findings indicate that 50 metabolites linked to 45 metabolic pathways were found to be significantly altered in the tested conditions. This study paves the way for the application of LC-MS-based metabolomics to understand the metabolism of MTB, leading to the development of processes to achieve enhanced production of magnetosomes.

2. Experimental

2.1 Chemicals and reagents

LC-MS grade methanol and acetonitrile were obtained from Fisher Scientific (Loughborough, UK) and VWR (West Sussex, UK), respectively. Ammonium carbonate, chemicals and all analytical standards were obtained from either Sigma-Aldrich (Gillingham, UK) or Fisher Scientific (Loughborough, UK) unless otherwise stated. Deionised water was prepared using a Milli-Q water purification system (Millipore, MA, USA). Five mixtures of 235 authentic standards were prepared at a concentration of 20 μM and used for the identification of the metabolites in the study. The list of the standards is available in Table S1 in the ESI.†

2.2 Strains, growth media and culture conditions of *Mgryph*

Mgryph MSR-1 was acquired from Deutsche Sammlung von Mikroorganismen und Zellkulturen GmbH culture collection (DSMZ, Braunschweig, Germany). Two types of *Mgryph* cells were obtained: (1) magnetosome and (2) non-magnetosome producing cells from microaerobic and aerobic bioreactor cultures, respectively, carried out under controlled conditions using a pH-stat fermentation strategy adapted from our previous study.[22] Both cell types were further re-suspended in 2 mL of phosphate-buffered saline (PBS), inoculated into 38 mL of Flask Standard Medium (FSM) and grown at 30 °C in a shaker incubator at 150 rpm for 48 h. Magnetosome producing cells ($n = 6$) were grown in airtight O_2-limited cultures while non-magnetosome producing cells ($n = 6$) were grown in aerobic cultures. The FSM was composed of 0.1 g L^{-1} yeast extract, 3 g L^{-1} soybean peptone, 3.5 g L^{-1} potassium L-lactate, 100 μM iron(III) citrate, 0.34 g L^{-1} $NaNO_3$, 0.1 g L^{-1} KH_2PO_4, 0.15 g L^{-1} $MgSO_4 \cdot 7H_2O$, 5 mL L^{-1} of EDTA-chelated trace element mixture and 2.38 g L^{-1} 4-(2-hydroxyethyl)piperazine-1-ethane sulfonic acid (HEPES) buffer in deionized water; adjusted to pH 7.0 prior to autoclave sterilisation.

2.3 Polyhydroxyalkanoates imaging using fluorescence microscopy

Mgryph cells (100 μL) were taken from FSM cultures and stained with 5 μL of 0.1 mg mL^{-1} of pyrromethene-546 (Pyr-546) in dimethyl sulfoxide for polyhydroxyalkanoates (PHAs) imaging. A Zeiss Primo Star iLed microscope (Carl Zeiss Ltd., Cambridge, UK) fitted with a Zeiss AxioCam ERc 5s camera was used. Images were acquired within 1 min of fluorophore incubation and processed with the aid of Zeiss ZEN Lite 2012 software in auto exposure mode. Samples were excited with a Zeiss Led 470 nm light source and a 515 LP filter was employed for detection of Pyr-546 fluorescence.

2.4 Measurement of cell concentration and cellular magnetism

Culture optical densities were recorded at a wavelength of 565 nm (OD_{565}) using an Evolution 300 UV-vis spectrophotometer controlled by Thermo Scientific™ VISIONpro™ software (Thermo Fisher Scientific, Hemel Hempstead, UK). Cellular magnetic response (C_{mag}) values were determined by OD_{565} measurements using a purpose-built magnetic measurement system mounted within the spectrophotometer as described elsewhere.[22] C_{mag} values greater than "1" indicate the presence of the magnetic cells.

2.5 Transmission electron microscopy

The bacterial samples (2 μL) were drop cast on a graphene oxide on lacey carbon supported 300 mesh copper grid (GOLC300Cu50, EM Resolutions, Sheffield, UK) and vacuum-dried before analysis. Transmission Electron Microscopy (TEM) images were obtained using a JEM-2100F microscope (JEOL, Herts, UK) operated at 200 kV equipped with a Gatan Orius CCD camera (Pleasanton, USA).

2.6 Sample preparation for LC-MS

Samples (1 mL) were taken after 48 h of cultivation and were immediately centrifuged at 10 000*g* for 3 min at 4 °C. The spent media were then separated from the cell pellets and kept at −80 °C for LC-MS-based metabolite profiling. The spent medium samples of magnetosome ($n = 6$), non-magnetosome producing cells ($n = 6$) of *Mgryph* and the control FSM ($n = 6$) were prepared for LC-MS as follows: an equal volume of the thawed medium on ice (50 μL) from each culture was added to an equal volume of methanol (50 μL) (1 : 1 sample : methanol), vortexed for 30 s, cooled on ice for 2 min, centrifuged at 10 000*g* at 4 °C for 5 min and analysed immediately. Reagent blanks ($n = 3$) were prepared using 1 : 1 water : methanol following the same procedure excluding the sample. For metabolomics analysis, a sample was prepared by mixing 20 μL from each sample in the study and used as a pooled QC sample.

2.7 Analytical methodologies: LC-MS for metabolite profiling and LC-MS/MS for metabolite identification

LC-MS analysis was performed using a Q-Exactive Plus mass spectrometer (MS) equipped with Dionex U3000 UHPLC system (Thermo Fisher Scientific, Hemel Hempstead, UK). Metabolites in the samples (5 μL, 4 °C) were separated on a ZIC-*p*HILIC column (4.6 × 150 mm, 5 μm particle size, Merck SeQuant, Watford, UK) in which the column was maintained at a flow rate of 300 μL min^{-1} at a temperature of 45 °C for 24 min as previously described.[23] The gradient started with 20% A (20 mM ammonium carbonate in water) and 80% of B (acetonitrile) and increased to 95% A over 15 min, then the composition was returned to its initial conditions in 2 min and the column was re-equilibrated for 7 min. The MS was operated in ESI+ and ESI− switching acquisition modes for LC-MS profiling of the samples and in data-dependent MS/MS (ddMS/MS) for identification for the analysis of the QC samples. For MS parameters, spray voltage was 4.5 kV (ESI+) and 3.5 (ESI−), and capillary voltage was 20 V (ESI+) and −15 V (ESI−). The sheath, auxiliary and sweep gas flow rates were 40, 5 and 1 (arbitrary unit), respectively, for both modes. Capillary and heater temperatures were maintained at 275 and 150 °C, respectively. Data were acquired for the LC-MS profiling with a resolution of 70 000 from *m*/*z* 70–1050. Top 5 ddMS/MS was performed on the QC sample ($n = 3$) at a resolution of 17 500 and a stepped normalised collision energy (NEC) of 20, 30 and 40.

The spent medium samples of the magnetosome, non-magnetosome producing cells and blank media (FSM, control) were randomised and analysed in a single LC-MS analytical run with the mixtures of authentic standards and reagent blanks. Pooled QC ($n = 6$) was injected at the beginning of the analysis to condition the column and after every 3–5 samples ($n = 6$) to check the stability, robustness, repeatability and performance of the analytical system.

2.8 Data analysis and metabolite identification

The acquired raw LC-MS datasets of the samples in the study were pre-processed for untargeted metabolomics, univariate analysis and metabolite identification with Compound Discoverer 3.1 SP1 software (Thermo Fisher Scientific, Hemel Hempstead, UK). Principal component analysis (PCA) and orthogonal partial least squares-discriminant analysis (OPLS-DA) were performed using Simca P+13 (Umetrics, Umeå, Sweden). The imported datasets were mean-centred and Pareto scaled. Cross-validation using the leave-one-out method was used to evaluate the robustness of the generated PCA and OPLS-DA by monitoring the fitness of model (R^2X) for PCA, (R^2Y) for OPLS-DA and predictive ability (Q^2) values.[24] Metabolite identification was performed using Compound Discoverer 3.1 SP1 software by matching accurate masses of the detected peaks with metabolites in *Mgryph* MSR-1 (MGRY1430440) BioCyc database, the retention times (RT) of the authentic standards (within 0.25 min shift) and *mz*Cloud fragmentation database. Briefly, retention time range used was 3.2–23.5 min, mass range was *m*/*z* 70–1050, mass tolerance for peak picking and metabolite identification was ≤ 5 ppm for precursor and fragment ions, minimum peak intensity was 1.0×10^6, intensity tolerance was at 30%, area max was greater or equal to 3.0×10^6, maximum retention time shift was 0.25 min and activation energy tolerance was 5. The confidence in metabolite identification was assigned as level 1–4 based on the recommendation by the Chemical Analysis Working Group, Metabolomics Standards Initiative (MSI).[25,26] In this classification, the metabolites identified using *m*/*z*, RT and/or MS/MS of reference standards were level 1, putatively annotated metabolites using *m*/*z*, RT and/or MS/MS from spectral library and no reference standards were level 2, putatively characterised metabolite classes were level 3 and unknowns were classified as level 4.

Variable importance in the projection (VIP) and |*p*(corr)| of the OPLS-DA were used to extract the metabolites responsible for the difference between the spent media of magnetosome and non-magnetosome producing cells. Student *t*-test adjusted with false discovery rate using the Benjamini–Hochberg

approach[27] for multiple testing problem were performed across all peak intensities detected in the samples.

2.9 Pathway analysis and metabolite network mapping

Pathway analysis, enrichment and network mapping of the significantly altered metabolites between magnetosome and non-magnetosome producing cells were performed using MetaboAnalyst 4.0.[28] The normalised abundances of the metabolites were Pareto scaled and processed for metabolite enrichment and pathway analysis while fold changes were used for KEGG metabolite network mapping.

3. Results and discussion

3.1 Comparison of physiological changes of *Mgryph* grown under O_2-limited and O_2-rich culture conditions

To characterise the physiological differences between *Mgryph* grown with O_2-rich and O_2-limited conditions, we used cryostocks from bioreactors using a pH-stat feeding strategy. Magnetic and non-magnetic cryostocks were prepared in 5% DMSO using cells harvested from a bioreactor experiment grown under microaerobic (pO_2 < 1%) and aerobic (pO_2 > 5%) conditions, respectively. Magnetic ($n = 6$) and non-magnetic ($n = 6$) cryostocks were inoculated into fresh FSM (control) and grown in O_2-limited and O_2-rich conditions (free air exchange), respectively, at 30 °C on a shaker incubator (150 rpm). Both cultures had headspace volumes of 20% and OD_{565} and C_{mag} were measured after 48 h. PHAs and magnetosome contents were also measured (Fig. 1). Cells grown under O_2-rich conditions grew better than O_2-limited conditions. It was confirmed that cells grown under O_2-rich conditions were not magnetic ($C_{mag} = 1$), whereas cells grown under O_2-limited conditions were magnetic ($C_{mag} = 1.82$) (Fig. 1A). Strong Pyr-546 fluorescence and electron microscopy images indicated the presence of large quantities of PHAs in both cultures (Fig. 1B and C). TEM analysis confirmed the presence and absence of magnetosome chains in the O_2-limited and O_2-rich cultures, respectively. These results are in agreement with findings from our previous studies:[29] using a 20% headspace volume allows relatively high

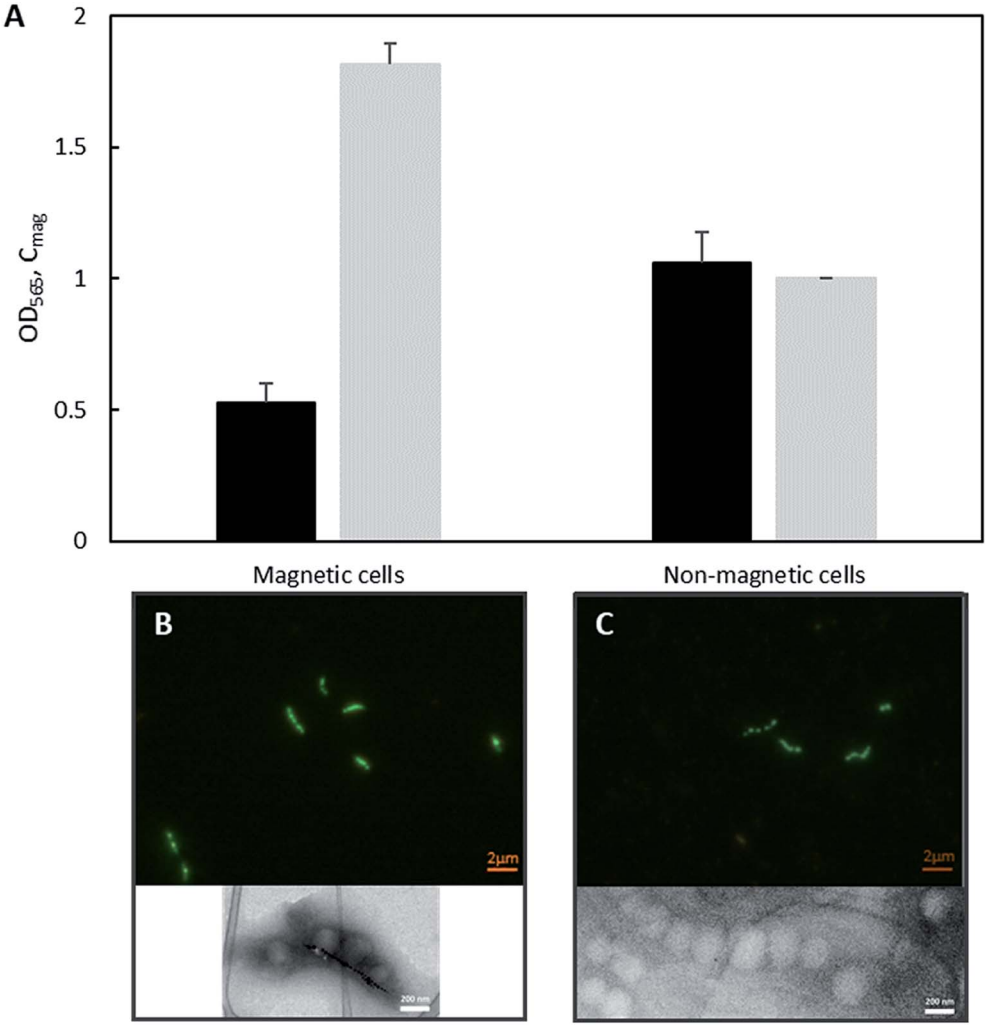

Fig. 1 Effect of O_2 limitation on the physiology of *Mgryph*. Cultures were grown under O_2-limited and O_2-rich conditions and characterised at 48 h. (A) OD_{565} (black bars) and cellular magnetism (C_{mag}; pale grey bars). Error bars are standard deviation ($n = 6$). Fluorescence of cells stained with Pyr-546 and transmission electron micrographs of magnetic (B) and non-magnetic (C) cells.

growth under free air exchange conditions, whereas it maintains the magnetic properties of *Mgryph* in shake flask cultures.[29] The presence of PHAs has been previously reported and might be due to the redirection of nutrients and energy competition between PHAs and magnetosome formation. In contrast, magnetosome formation is inhibited under aerobic conditions.[30]

3.2 Performance of LC-MS for untargeted metabolomics

The performance of the LC-MS-based metabolite profiling of the culture medium samples of magnetosome and non-magnetosome producing cells, and FSM (control medium sample) was assessed using univariate and multivariate analysis of all the detected peaks in the samples. The LC-MS datasets generated 2556 peaks in which the variability based on the use of relative standard deviations (RSDs) across the average peak areas was less than 30% for 93.3% of all peaks present in the QC. The variability in the QC was lower than the recommended threshold of RSD < 30% for at least 70% of all peaks for metabolomics analysis.[31] PCA was also used to assess the analytical performance of the method.[32,33] The pooled QCs were closely clustered towards the centre of the PCA scores plot (Fig. 2). These results demonstrate satisfactory instrumental stability and validate the LC-MS analytical performance for untargeted metabolomics.

3.3 Data analysis

The mass ion pairs (RT, *m*/*z*) from the dataset generated in this study were exported with their normalised abundances for multivariate analysis in which PCA and OPLS-DA were used for modelling the differences and similarities between samples. PCA was used to give an unbiased overview of any possible trends and clusters within the sample datasets. PCA-class analysis was first performed to evaluate the similarity of samples within each class. Tight clusters with no significant differences were observed within each class, indicated by the poor PCA-class Q^2 values (data not shown). This result demonstrates that the experimental setup, including the growth of microorganism, sample preparation and the analytical run, were carefully carried out, evidencing no outliers and adequate similarities within each class in the analysis.

Clear clustering and separation were observed in the metabolic profiles of the spent media of magnetosome and non-magnetosome producing cells, and FSM controls in both PCA and OPLS-DA scores plots (Fig. 2 and 3A). As can be seen in Fig. 3B, a further comparative OPLS-DA of the spent media of magnetosome and non-magnetosome producing cells showed that they were clearly separated and clustered, indicating that the metabolic profile is more distinct from one class into another. Cross-validation of this OPLS-DA was excellent with a cumulative R^2X of 0.76, R^2Y of 0.99 and Q^2 of 0.98; these values indicate that the models are less likely to be overfitted as they are higher than the recommended values of 0.50 of R^2X, R^2Y and Q^2 for a robust model.[24]

3.4 Feature selection and comparison of the significantly altered metabolites related to the presence of the magnetosomes

The 2556 metabolite features detected in the spent media of magnetosome compared to non-magnetosome producing cells (Fig. 4A) were submitted for metabolite identification using Compound Discoverer 3.1 SP1. The *m*/*z*, RT and/or MS/MS of these features were interrogated against the specific BioCyc database of *Mgryph*, the retention times (RT) of 235 authentic standards and the *mz*Cloud fragmentation database. 423 metabolites were identified in which only 137 metabolites were reported with high confidence in identification (*i.e.* Level 1 and 2 only) based on MSI levels of identification[25,26] as detailed earlier (Fig. 4B, Table S2 in the ESI†).

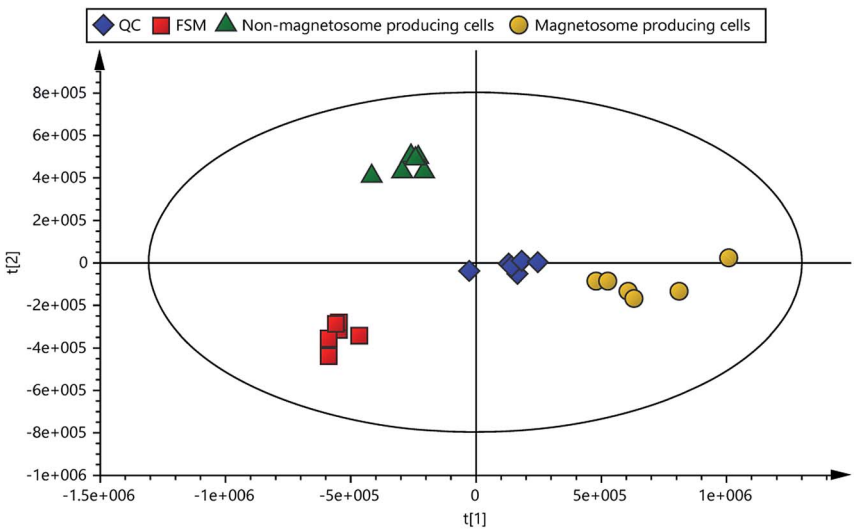

Fig. 2 PCA scores plot of FSM (flask standard media, control) and spent media of non-magnetosome (O_2-rich) and magnetosome-producing (O_2-limited) cells analysed with LC-MS (cross validation: $R^2X = 0.81$ and $Q^2 = 0.61$).

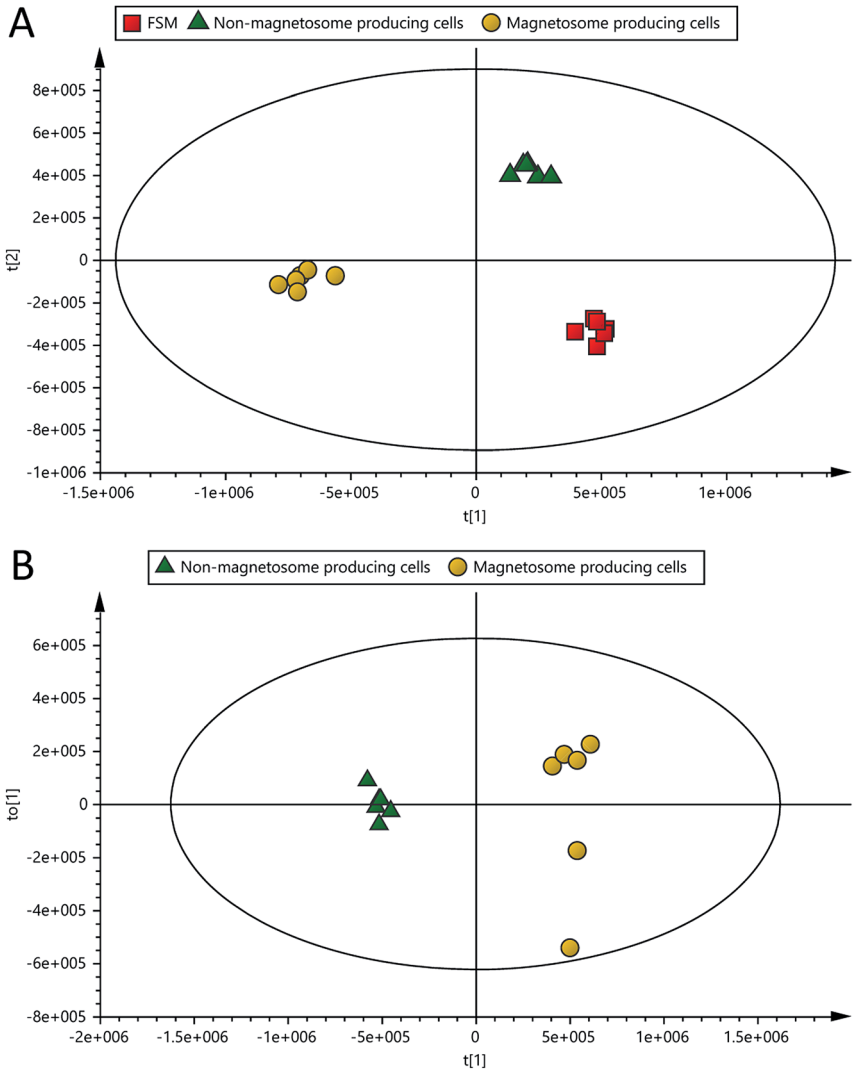

Fig. 3 OPLS-DA scores plots of the spent media of magnetosome (O_2-limited), non-magnetosome producing (O_2-rich) cells and FSM controls analysed with LC-MS (cross-validation: (A) $R^2X = 0.83$, $R^2Y = 0.99$ and $Q^2 = 0.96$; (B) $R^2X = 0.76$, $R^2Y = 0.99$ and $Q^2 = 0.98$).

The significantly altered metabolites in the samples were selected using both multivariate (OPLS-DA) and univariate analysis (adjusted *p*-values). VIP and |*p*(corr)| of the OPLS-DA were used to extract the metabolites relevant to the separation of samples in the model. VIP scores estimate the importance of each variable in the projection used in OPLS-DA and is often used for variable selection, while |*p*(corr)| reflects the reliability of each VIP score in the model.[34] Metabolites with adjusted *p*-value < 0.05, VIP > 1.0 and |*p*(corr)| > 0.4 were considered significantly altered metabolites (Fig. 4B). As a result, 50 metabolites, including amino acids, organic acids, energy molecules and nucleotides, were identified as significantly altered metabolites in the magnetosome- compared to non-magnetosome-producing cells. Fig. 5 shows a means of direct comparison of the levels of these metabolites; the full list of the key metabolites can be seen in Table S3 in the ESI.†

The level of AMP, lactate, pyruvate, acetoin, crotonate, pepicolate, trehalose and guanine were found to be high in the samples of magnetosome-producing cells compared to non-magnetosome producing cells (Table 1). This indicates that these metabolites were either excreted by *Mgryph* under the O_2-limited growth conditions or, if already present in the growth media, they were consumed at a slower rate compared to the O_2-rich cultures. The presence of higher level of lactate in the O_2-limited cultures compared to O_2-rich cultures is expected as it is the major carbon source component in FSM. The O_2-limited cultures showed lower biomass than the O_2-rich ones (Fig. 1A), hence, lower consumption of lactate. It is known that there is a correlation between *Mgryph* growth and lactate consumption.[22] On the other hand, the presence of acetoin could be related to its secretion under microaerobic growth conditions and this has been previously described to occur in *Bacillus subtilis*[35] grown under microaerobic conditions. The accumulation of AMP and pyruvate in the spent media of magnetosome-producing cells may suggest that lactate could be converted into pyruvate *via* lactate dehydrogenase and subsequently acetoin formation occurred *via* the pyruvate route.[36] Our results suggest that this may act as an alternative

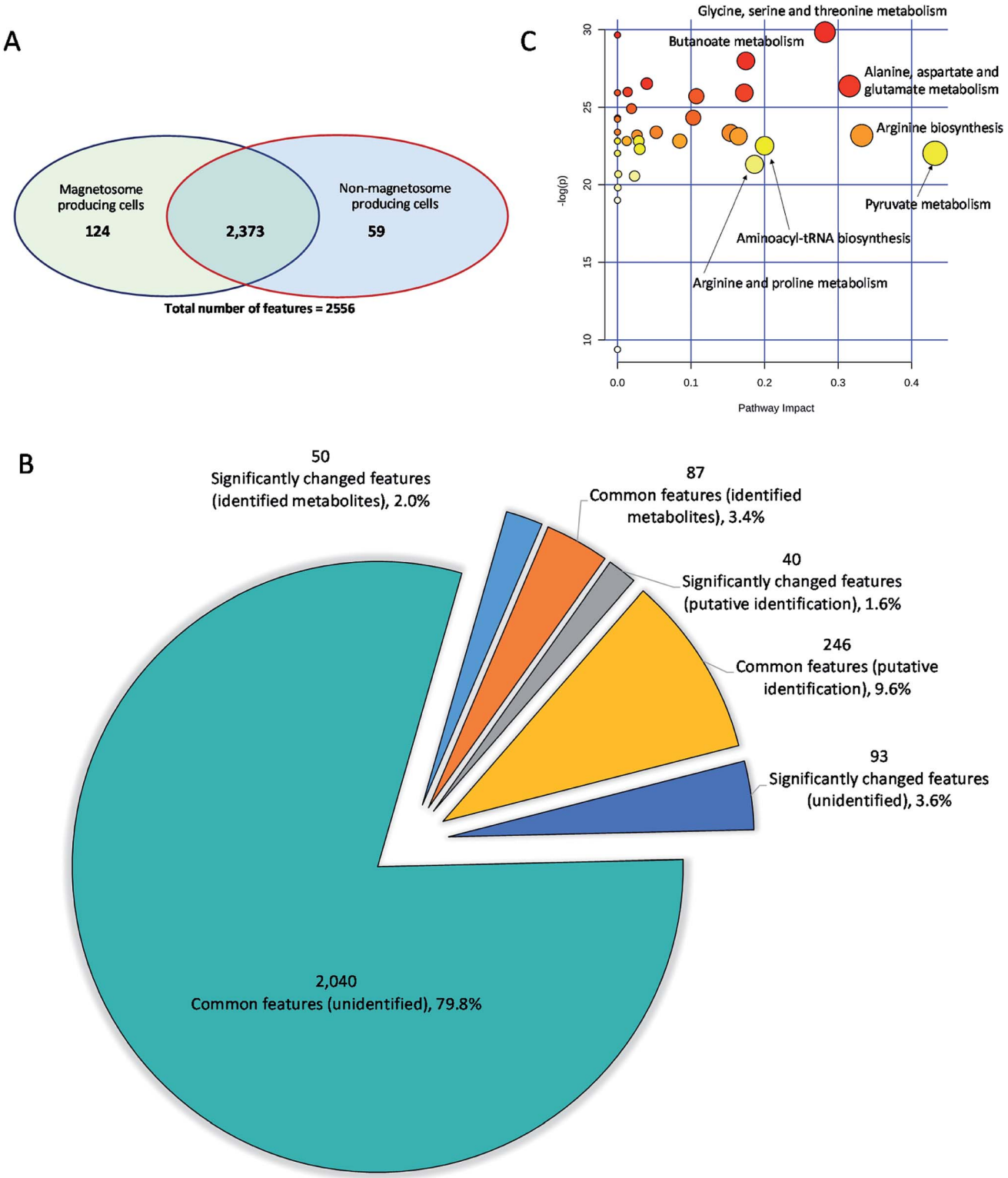

Fig. 4 Summary of the detected features, metabolite identification and pathway analysis of the significantly altered metabolites in the spent media of magnetosome compared to non-magnetosome producing cells. (A) Venn diagram presenting the common and the significantly changed features detected in the spent media samples, (B) pie-chart showing the significantly changed and the common number of identified metabolites (Level 1 and 2), putatively identified metabolites (Level 3 and 4) and the unidentified metabolite features between the two sets of samples; and (C) pathway analysis: the top pathways were ranked by the gamma-adjusted *p*-values for permutation per pathway (*y*-axis) and the total number of hits per pathway (*x*-axis). Colour graduated from white to yellow, orange and red, circle size (large > small) as well as the values of both *x* and *y* increase represents the degree of significance.

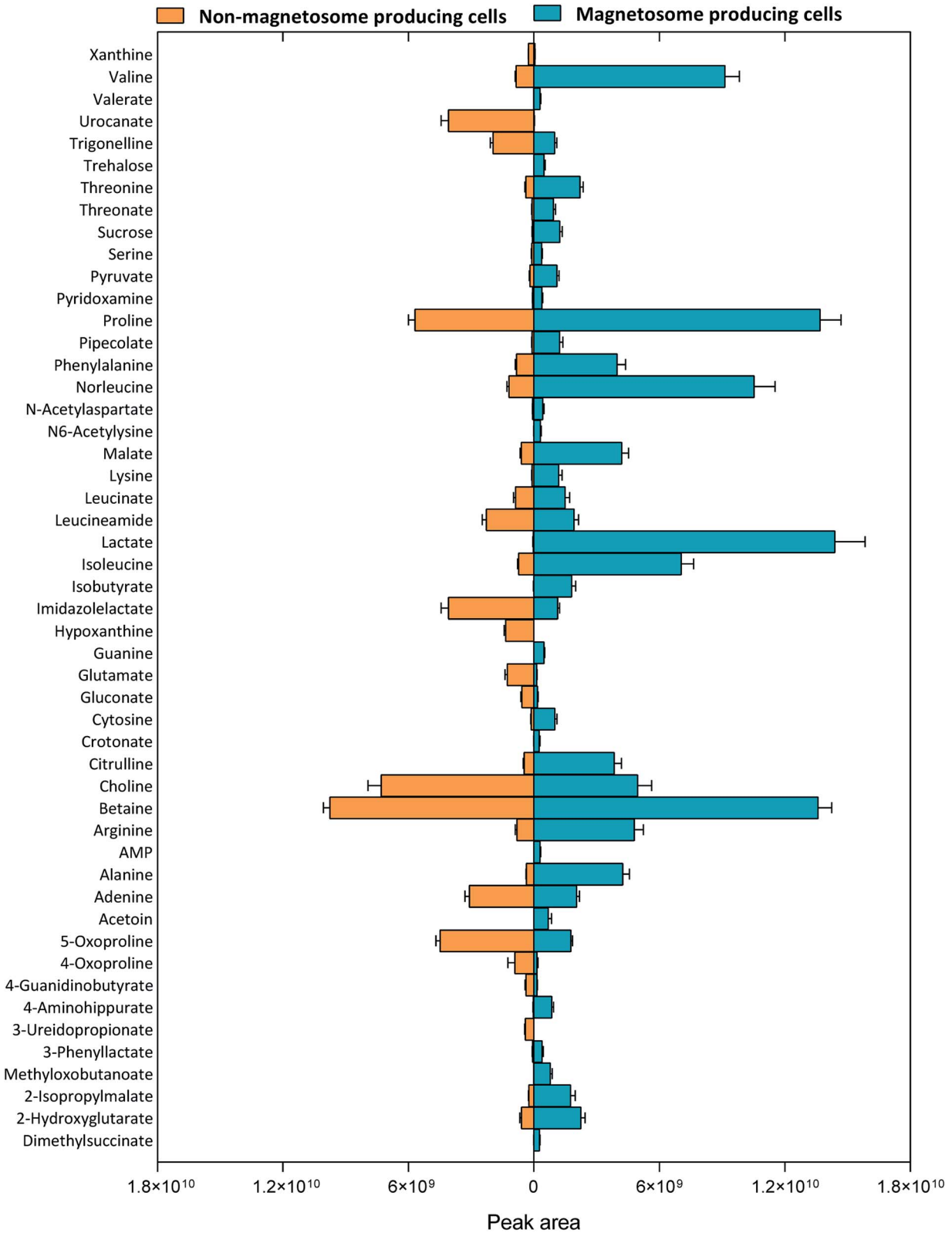

Fig. 5 Relative levels expressed as peak area (arbitrary units) of significantly altered metabolites in the spent media of *Mgryph* grown on O_2-limited cultures ($n = 6$, magnetosome producing cells) compared to O_2-rich cultures ($n = 6$, non-magnetosome producing cells).

energy and respiratory route during O_2-limited growth of *Mgryph*. In addition, pepicolate was also found to serve as an osmoprotector and support the growth of *E. coli* under stressed conditions[37] which may signal that *Mgryph* upregulated pepicolate to overcome its O_2-limited growth. This is further evident by the accumulation of trehalose in the

Table 1 The top significantly affected metabolites and metabolic pathways in the magnetosome producing cells compared to non-producing cells

Metabolite	Monoisotopic mass[a] (Da)	Formula	Identification[b]	Mass error (ppm)	log 2 fold change	Adjusted *p*-value[c]	OPLS-DA *p*(corr)	OPLS-DA VIP
(1) Metabolites								
AMP	347.0631	$C_{10}H_{14}N_5O_7P$	*m/z*, RT, MS/MS (1)	0.44	9.1	3.82×10^{-15}	1.00	1.17
Lactic acid	90.0317	$C_3H_6O_3$	*m/z*, RT, MS/MS (1)	1.93	8.4	3.82×10^{-15}	1.00	8.12
Trehalose	342.1165	$C_{12}H_{22}O_{11}$	*m/z*, MS/MS (2)	0.81	8.2	3.82×10^{-15}	0.99	1.50
Acetoin	88.0526	$C_4H_8O_2$	*m/z*, RT, MS/MS (1)	1.48	7.7	3.82×10^{-15}	0.96	1.75
Guanine	151.0495	$C_5H_5N_5O$	*m/z*, RT (1)	0.42	7.2	3.82×10^{-15}	0.99	1.50
Isobutyric acid	88.0526	$C_4H_8O_2$	*m/z*, MS/MS (2)	1.98	7.0	3.82×10^{-15}	0.99	2.87
2,2-Dimethylsuccinic acid	146.0581	$C_6H_{10}O_4$	*m/z*, MS/MS (2)	2.00	6.3	2.98×10^{-11}	0.99	1.10
N6-Acetylysine	188.1162	$C_8H_{16}N_2O_3$	*m/z*, RT	0.30	6.0	3.82×10^{-15}	0.99	1.20
Crotonic acid	86.0369	$C_4H_6O_2$	*m/z*, MS/MS (2)	1.87	5.9	3.82×10^{-15}	0.99	1.09
3-Methy-2-oxobutanoic acid	116.0476	$C_5H_8O_3$	*m/z*, RT, MS/MS (1)	2.01	5.2	3.82×10^{-15}	0.99	1.87
4-Aminohippuric acid	194.0691	$C_9H_{10}N_2O_3$	*m/z*, RT (1)	0.62	4.5	3.82×10^{-15}	0.99	1.94
Sucrose	342.1162	$C_{12}H_{22}O_{11}$	*m/z*, RT, MS/MS (1)	0.80	3.9	3.82×10^{-15}	1.00	2.31
Valeric acid	102.0683	$C_5H_{10}O_2$	*m/z*, MS/MS (2)	2.35	3.8	3.82×10^{-15}	0.99	1.13
Pipecolic acid	129.0790	$C_6H_{11}NO_2$	*m/z*, MS/MS (2)	0.58	3.6	3.82×10^{-15}	0.99	2.28
Lysine	146.1057	$C_6H_{14}N_2O_2$	*m/z*, RT (1)	0.34	3.6	3.82×10^{-15}	0.99	2.23
Alanine	89.0477	$C_3H_7NO_2$	*m/z*, RT, MS/MS (1)	0.30	3.5	3.82×10^{-15}	1.00	4.23
Valine	117.0790	$C_5H_{11}NO_2$	*m/z*, RT, MS/MS (1)	0.27	3.4	3.82×10^{-15}	1.00	6.17
Pyruvic acid	88.0162	$C_3H_4O_3$	*m/z*, MS/MS (2)	2.12	2.5	7.26×10^{-12}	0.99	2.05
Xanthine	152.0337	$C_5H_4N_4O_2$	*m/z*, RT, MS/MS (1)	1.52	−2.6	3.82×10^{-15}	−1.00	1.02
4-Oxoproline	129.0429	$C_5H_7NO_3$	*m/z*, MS/MS (2)	1.83	−2.7	6.89×10^{-7}	−0.88	1.78
Glutamate	147.0532	$C_5H_9NO_4$	*m/z*, RT, MS/MS (1)	0.25	−3.2	3.82×10^{-15}	−0.99	2.28
3-Ureidopropionic acid	132.0535	$C_4H_8N_2O_3$	*m/z*, MS/MS (2)	0.95	−6.9	3.82×10^{-15}	−0.99	1.38
Urocanic acid	138.0430	$C_6H_6N_2O_2$	*m/z*, MS/MS (2)	0.58	−7.6	3.82×10^{-15}	−0.99	4.34
Hypoxanthine	136.0386	$C_5H_4N_4O$	*m/z*, RT, MS/MS (1)	0.55	−8.6	3.82×10^{-15}	−0.99	2.49

Pathway	Total number of metabolites		*p*-value	log(*p*-value)	Adjusted *p*-value[c]	Pathway impact
	Pathway	Hits				
(2) Metabolic pathways						
Pyruvate metabolism	26	4	2.71×10^{-10}	22.03	3.23×10^{-10}	0.43
Arginine biosynthesis	16	3	8.61×10^{-11}	23.18	1.69×10^{-10}	0.33
Alanine, aspartate and glutamate metabolism	22	3	3.54×10^{-12}	26.37	2.46×10^{-11}	0.32
Glycine, serine and threonine metabolism	33	5	1.11×10^{-13}	29.83	2.98×10^{-12}	0.28
Aminoacyl-tRNA biosynthesis	45	10	1.68×10^{-10}	22.51	2.22×10^{-10}	0.2
Arginine and proline metabolism	29	3	5.56×10^{-10}	21.31	6.42×10^{-10}	0.19
Butanoate metabolism	17	2	7.08×10^{-13}	27.98	1.06×10^{-11}	0.17
D-Glutamine and D-glutamate metabolism	7	1	5.46×10^{-12}	25.93	2.46×10^{-11}	0.17
Valine, leucine and isoleucine biosynthesis	22	5	9.09×10^{-11}	23.12	1.69×10^{-10}	0.16
Methane metabolism	26	3	7.29×10^{-11}	23.34	1.69×10^{-10}	0.15
Glyoxylate and dicarboxylate metabolism	37	4	6.82×10^{-12}	25.71	2.79×10^{-11}	0.11
Purine metabolism	73	5	2.73×10^{-11}	24.33	8.46×10^{-11}	0.1

Table 1 (*Contd.*)

Pathway	Total number of metabolites		*p*-value	log(*p*-value)	Adjusted *p*-value[c]	Pathway impact
	Pathway	Hits				
(2) Metabolic pathways						
Glycolysis/gluconeogenesis	29	1	1.23×10^{-10}	22.82	1.69×10^{-10}	0.08
Citrate cycle (TCA cycle)	20	2	7.02×10^{-11}	23.38	1.69×10^{-10}	0.05
Pentose phosphate pathway	26	2	3.02×10^{-12}	26.53	2.46×10^{-11}	0.04

[a] Detected accurate mass. [b] Level of identification was based on MSI classification: (1) the metabolite was identified using *m/z*, RT and/or MS/MS of reference standards, (2) the metabolite was putatively annotated using *m/z*, RT and/or MS/MS from spectral library and no reference standards, (3) metabolite class was putatively characterised and (4) unknowns. [c] *p*-Values were adjusted using Benjamini Hochberg FDR.

samples of magnetosome producing cells as endogenous trehalose was found to play an important role as an osmo- and stress-protector in *E. coli*.[38] For further understanding of the metabolic changes in *Mgryph* during the formation of the magnetosomes, the list of significant metabolites was submitted for pathway analysis.

3.5 Pathway analysis and metabolite network mapping

The significantly changed metabolites identified by comparing the magnetosome and non-magnetosome producing *Mgryph* cells were submitted for pathway analysis and network mapping using MetaboAnalyst 4.0.[28] More than 40 metabolic pathways were found significantly affected in the magnetosome compared to non-magnetosome producing cells (Table S4 in the ESI†) in which glycine, serine and threonine; butanoate; alanine, aspartate and glutamate; aminoacyl-tRNA biosynthesis; and pyruvate and TCA metabolisms were highly affected (Fig. 4C, Table 1). Pathway network mapping in Fig. S1 in the ESI† highlighted the most significantly altered metabolite interactions. The map depicts interacting metabolites across the metabolic pathways identified through specific base-pair alignment. As can be observed in Fig. S1 in the ESI,† L-glutamic acid, pyruvic acid and adenosine monophosphate are the key metabolites showing the highest number of metabolite interactions across the metabolic networks.

3.6 The magnetosome and the amino acid metabolism

Amino acids are key carbon and energy sources for the growth of magnetotactic bacteria.[22] They are essential for the growth of *Mgryph* and usually supplied in the culture using yeast extract which are rich in amino acids. Previous works showed that *Mgryph* was not be able to sustain growth above 1.5 OD_{565} when yeast extract was not included in the culture (not published). Such growth under limited amino acid source was approximately 10-fold lower than the highest biomass concentration reached in *Mgryph*.[22] The levels of glutamine, ornithine, hypoxanthine, tryptophan, serine, phenylalanine, glycine, glutamate, 2-oxoglutarate and aspartate were found lower in the magnetosome producing cells compared to fresh media (FSM) (Fig. 6, Table S2 in the ESI†) indicating that these amino acids and their metabolites were significantly utilised during microaerobic growth of *Mgryph*. FSM contains large quantities of yeast extract and peptone, as detailed in the experimental section, necessary for the growth of *Mgryph*. Among all amino acids present in FSM, glutamate appeared to be slightly utilised in O_2-rich growth conditions whilst it was heavily consumed under O_2-limited conditions (Fig. 6, an enlarged version of the pathway map is also available in Fig. S2 in the ESI†), hence glutamate utilisation might be potentially linked to the formation of magnetosomes.

To further understand the decrease of amino acids in the O_2-limited growth conditions in comparison to fresh FSM, it is necessary to take into account the proteome associated to magnetosomes and their formation: the conserved genomic magnetosome island (MAI) in *Mgryph* comprises 28 genes and

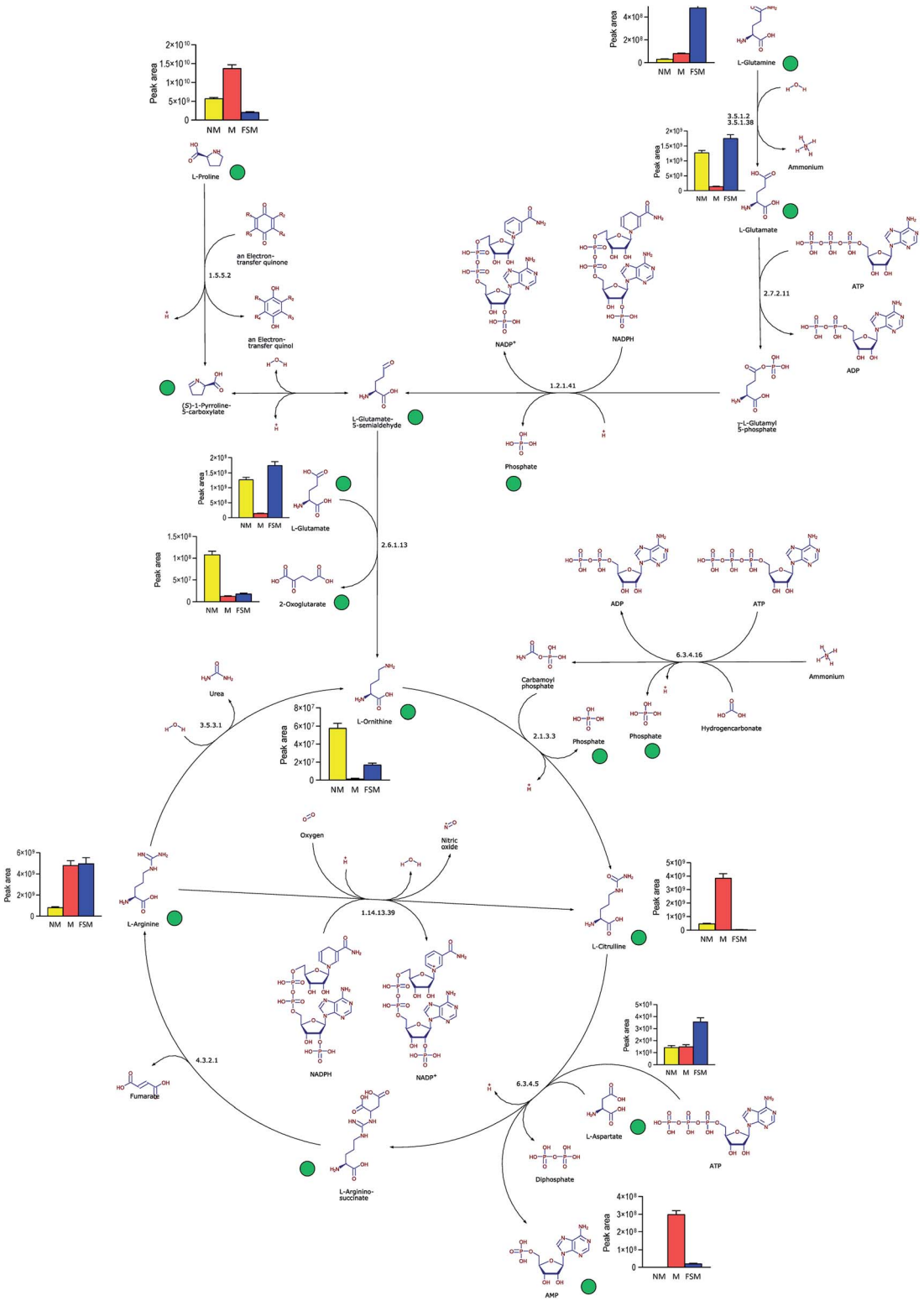

Fig. 6 Pathway mapping of metabolites detected in the spent medium samples of non-magnetosome (NM), magnetosome (M) producing *Mgryph* cells and control FSM. Green circle indicates that the metabolite was detected in the samples while the bar graph shows the relative abundance of metabolites expressed as peak areas (arbitrary units).

their associated proteins which are involved in the magnetosome formation.[8,39] This cellular machinery is "switched on" under microaerobic conditions.[3] Therefore, lower levels of the amino acids, listed above, may indicate that these were utilised in the anabolic metabolism and synthesis of magnetosome-related proteins for structural or enzymatic purposes. Interestingly, it has been previously reported that aspartate, glutamate, proline and serine were the only amino acids significantly

utilised by ε-proteobacteria *Campylobacter jejuni* during microaerobic growth.[40] Also, the authors reported that the growth of an aspartase (aspA) mutant of *Campylobacter jejuni* (unable to utilise any amino acid except serine) and a Cj0762c (aspB) mutant (unable to utilise glutamate), were severely impaired. Recently, microaerobic growth conditions were found to upregulate amino acid synthesis genes in *E. coli*.[41] Our findings, therefore, may indicate that the glycine, serine and threonine, and alanine, aspartate and glutamate metabolisms might be linked to the enhanced utilisation of these amino acids by *Mgryph* under O_2-limited growth conditions where magnetosomes were formed.

3.7 Protein biosynthesis in *Mgryph*

Aminoacyl-tRNAs are substrates for translation and are pivotal in determining how the genetic code is interpreted as amino acids, thus playing an important role in protein synthesis.[42] Aminoacyl-tRNA biosynthesis pathways were significantly enhanced in the magnetosome producing culture, suggesting that they may be related to the biosynthesis of some proteins involved in magnetosome formation. These proteins may include those associated with the complex enzymatic and structural machinery in the iron biomineralisation and the formation of the magnetosome membrane which involves approximately 30 genes.[43]

3.8 Butyrate metabolism in *Mgryph*

Butanoate (butyrate) metabolism was significantly altered under O_2-limited conditions in comparison to O_2-rich conditions (Fig. 4C) and describes the metabolic fate of a number of short chain fatty acids/alcohols. Butanoate metabolism is linked to the formation of hydroxybutyrate, butyrate, acetone, succinate and crotonate. The butanoate metabolism is typically active in a variety of microorganisms that grow under microaerobic or anaerobic conditions, such as the obligate anaerobe *Clostridium butyricum*[44] or lactic acid bacteria.[45] As shown in Fig. 1, both cultures grown under O_2-limited and O_2-rich conditions accumulated large aggregates of PHAs consistent with previous studies in which limiting N_2 and O_2 under carbon excess resulted in high-level accumulation of PHAs in different bacteria species.[46,47] Similar behaviour was also observed in our previous studies,[29] whereby the relative content of PHAs decreased in microaerobic cultures after 48 h suggesting that *Mgryph* utilised PHAs as substrate. Therefore, the significant increase in the butanoate metabolism may indicate that PHAs were significantly utilised in the O_2-limited cultures whereas the O_2-rich cultures showed lower metabolism by this route.

4. Conclusion

In this study, metabolic characterisation of *Mgryph* spent media has been performed in magnetosome and non-magnetosome producing conditions using LC-MS. This led to the identification of differentially regulated metabolites in more than 40 metabolic pathways. Our findings indicate that these significant metabolic changes are possibly related to the energy and anabolic metabolism necessary for the growth, the degradation of PHAs and the synthesis of proteins involved in the formation of magnetosomes. This study will play a critical role in improving the understanding of the underlying metabolic mechanisms in *Mgryph*. Combined with stable isotope assisted approaches,[18,48,49] this study can be extended to quantify the intracellular metabolite fluxes in specific stages of *Mgryph* growth, thus contributing to the further understanding of the metabolic mechanisms that affect the cell growth and the magnetosomes formation. In the long term, we envisage that the significant improvement of both, *Mgryph* growth and magnetosome production will depend to a large extend, in the application and combination of "omics" technologies along with high-yield bioprocessing strategies. This combination will ultimately accelerate the development of magnetosome-based products in a wide range of biotechnology and nanomedicine, such as drug delivery, magnetic hyperthermia and diagnostic applications.

Conflicts of interest

The authors declare no competing financial interest.

Acknowledgements

This work was supported by the NanoPrime EPSRC grant EP/R025282/1; Royal Society Research grant RGS\R1\191377; the Aston Institute of Materials Research (AIMR) Seed-corn grant; the Energy Research Accelerator (ERA) grant from Innovate UK and the Green Chemicals Beacon of Excellence, University of Nottingham. The authors acknowledge the assistance of the visiting student Jonathan Andraud of the Université Clermont Auvergne for the pre-culture experiments; and Tim W Overton and Owen RT Thomas of the University of Birmingham for enabling the access to the C_{mag} measurement system.

References

1 D. L. Balkwill, D. Maratea and R. P. Blakemore, *J. Bacteriol.*, 1980, **141**, 1399–1408.
2 N. A. Frey, S. Peng, K. Cheng and S. Sun, *Chem. Soc. Rev.*, 2009, **38**, 2532–2542.
3 U. Heyen and D. Schüler, *Appl. Microbiol. Biotechnol.*, 2003, **61**, 536–544.
4 S. Wilhelm, A. J. Tavares, Q. Dai, S. Ohta, J. Audet, H. F. Dvorak and W. C. W. Chan, *Nat. Rev. Mater.*, 2016, **1**, 16014.
5 I. Fischer, C. C. Hsu, M. Gärtner, C. Müller, T. W. Overton, O. R. Thomas and M. Franzreb, *J. Chromatogr. A*, 2013, **1305**, 7–16.
6 P. Tajer-Mohammad-Ghazvini, R. Kasra-Kermanshahi, A. Nozad-Golikand, M. Sadeghizadeh, S. Ghorbanzadeh-Mashkani and R. Dabbagh, *Bioprocess Biosyst. Eng.*, 2016, **39**, 1899–1911.
7 K. Grünberg, E. C. Müller, A. Otto, R. Reszka, D. Linder, M. Kube, R. Reinhardt and D. Schüler, *Appl. Environ. Microbiol.*, 2004, **70**, 1040–1050.

8 R. Uebe and D. Schüler, *Nat. Rev. Microbiol.*, 2016, **14**, 621–637.
9 A. Fernández-Castané, H. Li, O. R. T. Thomas and T. W. Overton, *New Biotechnol.*, 2018, **46**, 22–30.
10 F. Guo, Y. Liu, Y. Chen, T. Tang, W. Jiang, Y. Li and J. Li, *Appl. Microbiol. Biotechnol.*, 2011, **90**, 1277–1283.
11 Y. Zhang, X. Zhang, W. Jiang, Y. Li and J. Li, *Appl. Environ. Microbiol.*, 2011, **77**, 5851–5856.
12 A. Lohße, I. Kolinko, O. Raschdorf, R. Uebe, S. Borg, A. Brachmann, J. M. Plitzko, R. Müller, Y. Zhang and D. Schüler, *Appl. Environ. Microbiol.*, 2016, **82**, 3032–3041.
13 T. Suzuki, Y. Okamura, A. Arakaki, H. Takeyama and T. Matsunaga, *FEBS Lett.*, 2007, **581**, 3443–3448.
14 E. Ozyamak, J. Kollman, D. A. Agard and A. Komeili, *J. Biol. Chem.*, 2013, **288**, 4265–4277.
15 T. Wen, F. Guo, Y. Zhang, J. Tian, Y. Li, J. Li and W. Jiang, *Sci. Rep.*, 2016, **6**, 21156.
16 A. Abuawad, C. Mbadugha, A. M. Ghaemmaghami and D.-H. Kim, *Metabolomics*, 2020, **16**, 33.
17 M. S. Nadeem, M. Razeeth, H. M. Z. Choudhry, F. Anwar, M. A. Zamzami, B. N. Murtaza, F. A. M. Al-Abbasi, M. I. Khan and A. R. Shakoori, *J. Cell. Biochem.*, 2020, **121**, 125–134.
18 S. Schatschneider, S. Abdelrazig, L. Safo, A. M. Henstra, T. Millat, D.-H. Kim, K. Winzer, N. P. Minton and D. A. Barrett, *Anal. Chem.*, 2018, **90**, 4470–4477.
19 F. R. Pinu and S. G. Villas-Boas, *Metabolites*, 2017, **7**, 43.
20 J. Kim, Y. E. Cheong, I. Jung and K. H. Kim, *Mar. Drugs*, 2019, **17**, 82.
21 N. A. Herman, S. J. Kim, J. S. Li, W. Cai, H. Koshino and W. Zhang, *Nat. Commun.*, 2017, **8**, 1514.
22 A. Fernández-Castané, H. Li, O. R. T. Thomas and T. W. Overton, *New Biotechnol.*, 2018, **46**, 22–30.
23 A. Surrati, R. Linforth, I. D. Fisk, V. Sottile and D. H. Kim, *Analyst*, 2016, **141**, 3776–3787.
24 L. Eriksson, E. Johansson, N. Kettaneh-Wold, C. W. J. Trygg and S. Wold, *Multi- and Megavariate Data Analysis: Basic Principles and Applications, Umetrics AB*, Umea, 2nd edn, 2006.
25 L. W. Sumner, A. Amberg, D. Barrett, M. H. Beale, R. Beger, C. A. Daykin, T. W. M. Fan, O. Fiehn, R. Goodacre, J. L. Griffin, T. Hankemeier, N. Hardy, J. Harnly, R. Higashi, J. Kopka, A. N. Lane, J. C. Lindon, P. Marriott, A. W. Nicholls, M. D. Reily, J. J. Thaden and M. R. Viant, *Metabolomics*, 2007, **3**, 211–221.
26 L. W. Sumner, Z. Lei, B. J. Nikolau, K. Saito, U. Roessner and R. Trengove, *Metabolomics*, 2014, **10**, 1047–1049.
27 Y. Benjamini and Y. Hochberg, *J. R. Stat. Soc. Ser. B Methodol.*, 1995, **57**, 289–300.
28 J. Chong, D. S. Wishart and J. Xia, *Curr. Protoc. Bioinf.*, 2019, **68**, e86.
29 A. Fernández-Castané, H. Li, O. R. T. Thomas and T. W. Overton, *Sci. Rep.*, 2017, **7**, 13118.
30 X. Wang, H. Zheng, Q. Wang, W. Jiang, Y. Wen, J. Tian, J. Sun, Y. Li and J. Li, *Front. Microbiol.*, 2019, **10**, 1478.
31 O. Begou, H. G. Gika, G. A. Theodoridis and I. D. Wilson, in *Metabolic Profiling: Methods and Protocols*, ed. G. A. Theodoridis, H. G. Gika and I. D. Wilson, Springer New York, New York, NY, 2018, pp. 15–26, DOI: 10.1007/978-1-4939-7643-0_2.
32 E. J. Want, I. D. Wilson, H. Gika, G. Theodoridis, R. S. Plumb, J. Shockcor, E. Holmes and J. K. Nicholson, *Nat. Protoc.*, 2010, **5**, 1005–1018.
33 H. G. Gika, G. A. Theodoridis, J. E. Wingate and I. D. Wilson, *J. Proteome Res.*, 2007, **6**, 3291–3303.
34 P. Yin, D. Wan, C. Zhao, J. Chen, X. Zhao, W. Wang, X. Lu, S. Yang, J. Gu and G. Xu, *Mol. BioSyst.*, 2009, **5**, 868–876.
35 M. Wang, J. Fu, X. Zhang and T. Chen, *Biotechnol. Lett.*, 2012, **34**, 1877–1885.
36 J. Zhu, A. Sánchez, G. N. Bennett and K.-Y. San, *Metab. Eng.*, 2011, **13**, 704–712.
37 G. Gouesbet, M. Jebbar, R. Talibart, T. Bernard and C. Blanco, *Microbiology*, 1994, **140**, 2415–2422.
38 A. R. Strøm and I. Kaasen, *Mol. Microbiol.*, 1993, **8**, 205–210.
39 K. Grünberg, E.-C. Müller, A. Otto, R. Reszka, D. Linder, M. Kube, R. Reinhardt and D. Schüler, *Appl. Environ. Microbiol.*, 2004, **70**, 1040–1050.
40 E. Guccione, R. Leon-Kempis Mdel, B. M. Pearson, E. Hitchin, F. Mulholland, P. M. van Diemen, M. P. Stevens and D. J. Kelly, *Mol. Microbiol.*, 2008, **69**, 77–93.
41 K. Pandi, A. S. Chauhan, J. A. Gupta and A. S. Rathore, *Appl. Microbiol. Biotechnol.*, 2020, **104**(13), 5773–5785.
42 M. Ibba and D. Soll, *Annu. Rev. Biochem.*, 2000, **69**, 617–650.
43 O. Raschdorf, Y. Forstner, I. Kolinko, R. Uebe, J. M. Plitzko and D. Schüler, *PLoS Genet.*, 2016, **12**, e1006101.
44 M. Salmela, T. Lehtinen, E. Efimova, S. Santala and R. Mangayil, *Biotechnol. Biofuels*, 2018, **11**, 187.
45 G. A. M. Cresci, P. C. Mayor and S. A. Thompson, *FEMS Microbiol. Lett.*, 2017, 364.
46 A. C. Ward, B. I. Rowley and E. A. Dawes, *Microbiology*, 1977, **102**, 61–68.
47 B. Kessler and B. Witholt, *J. Biotechnol.*, 2001, **86**, 97–104.
48 D.-H. Kim, F. Achcar, R. Breitling, K. E. Burgess and M. P. Barrett, *Metabolomics*, 2015, **11**, 1721–1732.
49 D. J. Creek, M. Mazet, F. Achcar, J. Anderson, D. H. Kim, R. Kamour, P. Morand, Y. Millerioux, M. Biran, E. J. Kerkhoven, A. Chokkathukalam, S. K. Weidt, K. E. Burgess, R. Breitling, D. G. Watson, F. Bringaud and M. P. Barrett, *PLoS Pathog.*, 2015, **11**, e1004689.

